

Designing of an Induction Motor Drive and Controller – Vector Control Approach

Abdulazeez Adebayo OLAYINKA - 20626477
 Electrical and Electronics Engineering
 University of Nottingham
 Nottingham, United Kingdom
eexao22@nottingham.ac.uk

Dr. Tabish Nazir MIR – Module Convenor
 Electrical and Electronics Engineering
 University of Nottingham
 Nottingham, United Kingdom
tabish.mir@nottingham.ac.uk

I. INTRODUCTION

This report is the continuation of [1] [2] where adopted motor parameters are given in Table I. This report discussed the vector-controlled drive for this induction motor. Section II presents the minimum DC link voltage required to control the drive and the device ratings while Section III discusses the current and speed controllers for this drive Section IV shows the MATLAB implementation of indirect vector control of this motor with feed-forward compensation. while Section V presents additions of field weakening control parametric drift in rotor resistance control (online rotor time constant estimator).

Table I: Three-Phase, 4-Pole, Squirrel Cage Induction Motor

| Parameter | Value | Parameter | Value |
|-----------------------------|-------------------------|-------------------------------------|----------------------|
| Power Rating | 2.2 kW | Voltage Rated (L-L) | 230 V, 50Hz |
| Stator Resistance (R_s) | 2.73 Ω | Rated Speed | 1435 rpm |
| Rotor Resistance (R_r) | 0.7 Ω | Stator Leakage Inductance (l_s) | 4.9 mH |
| Mutual Inductance (L_m) | 284 mH | Rotor Leakage Inductance (l_r) | 4.9 mH |
| Inertia (J) | 0.0103 kgm ² | Friction Factor (B) | 1.5×10^{-4} |

II. DC LINK VOLTAGE AND DEVICE SELECTION

The drive is fed from a three-phase voltage source inverter (VSI) with sinusoidal pulse width modulation. To obtain the minimum DC link voltage, the linear region of the plot of the ratio of fundamental line-to-line voltage to the DC link of the VSI against the amplitude modulation ratio (modulation index) [3] [4] as shown in Figure 1 is used to obtain the DC link voltage. The fundamental pole voltage is calculated in Equation 1 and the minimum DC link voltage in Equation 2. A 0.89 modulation index is assumed for this design.

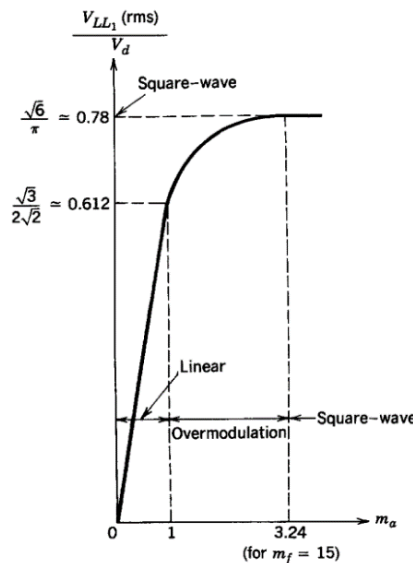


Figure 1: Three Phase Inverter – $V_{LL}(rms)/V_d$ against m_a [3]

$$\hat{V}_{A01} = \frac{\sqrt{2}V_{LL1}}{\sqrt{3}} = \frac{\sqrt{2} \times 230}{\sqrt{3}} = 187.794 V \dots \dots 1$$

$$V_d = \frac{2\hat{V}_{A01}}{m} = \frac{2 \times 187.794}{0.89} = 422.009 \text{ V} \dots \dots \dots 2$$

• **Device Selection**

The minimum blocking voltage for the switches is **422.009 V** (OFF state blocking) while the minimum continuous current is **8.7 A** (ON state continuous current).

An STMicroelectronics STGP10NC60KD IGBT with **20 A** rated current and **600 V** rated voltage, 3-Pin, through-hole is selected for this design and the datasheet can be found at [5]. At **100°C** this device can operate at **10 A** making this a good rating for the induction motor drive. The price for this device is **£0.817** (VAT included) at [6] with special application for induction motor drives [5] making it a very good candidate for this design.

III. DESIGN OF VECTOR CONTROLLER GAINS

The current loop gain (red colour) and speed loop gain (black colour) as shown in Figure 2 are discussed in this section to be implemented on MATLAB Simulink as presented in the next section. A saturation of 250% of the rated values of each output signal of the controllers was implemented in this design.

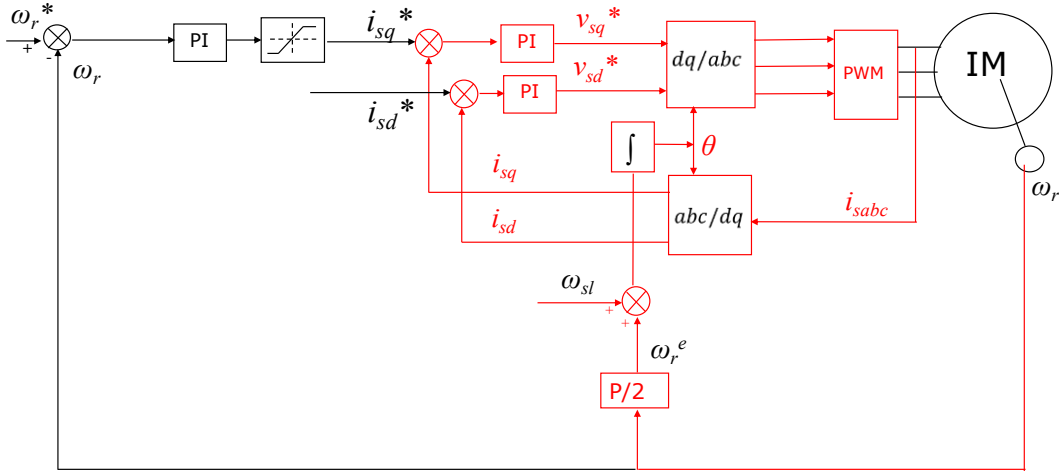


Figure 2: Indirect Vector Control of the Induction Motor with RFO [2] [7]

• **Current Controller Design**

Considering the stator dynamics Equations 3 and 4 in the dq reference frame, considering the first two terms, the plant Transfer Function is derived as in Equations 5 and 6 in the frequency domain.

$$v_{sd} = R_s i_{sd} + \sigma L_s \frac{d}{dt} i_{sd} - \omega_e \sigma L_s i_{sq} + \frac{L_m}{L_r} \frac{d}{dt} \phi_{rd} \dots \dots \dots 3$$

$$v_{sq} = R_s i_{sq} + \sigma L_s \frac{d}{dt} i_{sq} + \omega_e \sigma L_s i_{sd} + \omega_e \frac{L_m}{L_r} \phi_{rd} \dots \dots \dots 4$$

$$i_{sd} = \frac{1}{(s\sigma L_s + R_s)} v_{sd} \dots \dots \dots 5 \text{ from } 3$$

$$i_{sq} = \frac{1}{(s\sigma L_s + R_s)} v_{sq} \dots \dots \dots 6 \text{ from } 4$$

Therefore, both the d-axis and q-axis components of the current loops have the same transfer function.

While neglecting the delay caused by the inverter and anti-aliasing filter due to their very low time delay as compared to the plant, then the current control feedback block is given in Figure 3.

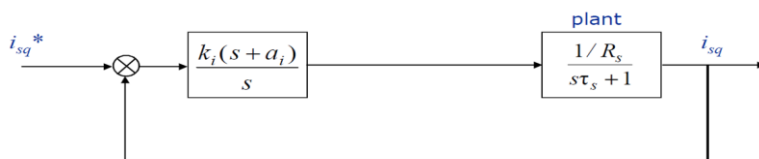


Figure 3: Current Controllers Block Diagram [2] [7]

Where the first block is the PI controller with k_i proportional gain and $\frac{k_i a_i}{s}$ integral gain. The close loop transfer function is derived from Equations 7 to 14.

$$\tau_s = \sigma \frac{L_s}{R_s} \dots \dots \dots 7$$

$$p = \frac{1}{\tau_s} \dots \dots \dots 8$$

$$k = \frac{1/R_s}{\tau_s} \dots \dots \dots 9$$

$$G_{plant} = \frac{k/p}{s/p + 1} \dots \dots \dots 10$$

$$G_{ctrl} = \frac{k_i(s + a_i)}{s} \dots \dots \dots 11$$

$$G_{cl} = \frac{G_{plant}G_{ctrl}}{1 + G_{plant}G_{ctrl}} \dots \dots \dots 12$$

$$G_{plant}G_{ctrl} = \frac{k/p}{s/p + 1} \times \frac{k_i(s + a_i)}{s} = \frac{kk_i(s + a_i)}{s^2 + sp} \dots \dots \dots 13$$

$$G_{cl} = \frac{\frac{kk_i(s + a_i)}{s^2 + p}}{1 + \frac{kk_i(s + a_i)}{s^2 + sp}} = \frac{kk_i(s + a_i)}{s^2 + sp} \times \frac{s^2 + sp}{s^2 + sp + kk_i(s + a_i)} = \frac{kk_i(s + a_i)}{s^2 + s(p + kk_i) + kk_i a_i} \dots \dots \dots 14$$

Comparing the closed-loop transfer function in Equation 14 to the second-order frequency equation gives rise to Equation 15.

$$\frac{kk_i(s + a_i)}{s^2 + (p + kk_i)s + kk_i a_i} = \frac{kk_i(s + a_i)}{s^2 + 2\zeta\omega_n s + \omega_n^2} \dots \dots \dots 15$$

For the current controller of this design, the natural frequency for the current loops is 200Hz while the damping factor was selected to be 1. $\omega_n = 2\pi f = 1256.637 \text{ rad/s}$ and $\zeta = 1$. The leakage coefficient (σ) is given in Equation 16 and the stator time constant (τ_s) is calculated as in Equation 17. Then p and k are calculated in Equations 18 and 19 respectively.

$$\sigma = \frac{l_s}{L_m} = 0.017 \dots \dots \dots 16$$

$$\tau_s = \sigma \frac{l_s + L_m}{R_s} = 0.00183 \text{ s} \dots \dots \dots 17$$

$$p = \frac{1}{\tau_s} = 547.693 \text{ s}^{-1} \dots \dots \dots 18$$

$$k = \frac{1/R_s}{\tau_s} = 200.620 \dots \dots \dots 19$$

Comparing the denominators of Equation 15.

$$s^2 + (547.693 + 200.62k_i)s + 200.62k_i a_i = s^2 + 2513.274s + 1256.637^2$$

$$s^1: 547.693 + 200.62k_i = 2513.274$$

$$k_i = 9.798 \dots \dots \dots 20$$

$$s^0: 200.62k_i a_i = 1256.637^2$$

$$a_i = 803.394 \dots \dots \dots 21$$

Therefore, from the controller block, proportional and integral are calculated as in Equations 22 and 23 respectively.

$$KP = k_i = 9.798 \dots \dots \dots 22$$

$$KI = k_i a_i = 7871.274 \dots \dots 23$$

Then, the current controller gain becomes

$$G_{ctrl} = \frac{9.798(s + 803.394)}{s}$$

• **Speed Controllers Design**

The closed-loop control block diagram is derived from Figure 2 as shown in Figure 4.

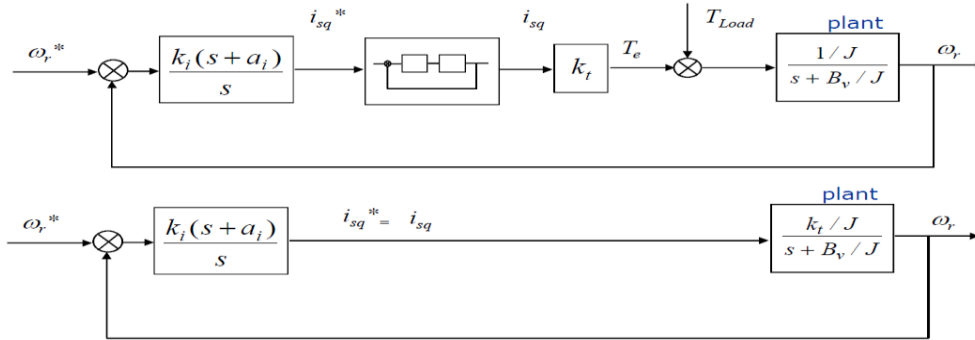


Figure 4: Speed Controllers Block Diagram [2] [7]

The closed-loop transfer function is derived from Equations 24 to 28.

$$G_{plant} = \frac{k_t/J}{s + B/J} \dots \dots 24$$

Let

$$k_j = \frac{k_t}{J} \dots \dots 25$$

$$B_j = \frac{B}{J} \dots \dots 26$$

Then

$$G_{plant}G_{ctrl} = \frac{k_j}{s + B_j} \times \frac{k_i(s + a_i)}{s} = \frac{k_j k_i (s + a_i)}{s + B_j} \dots \dots 27$$

Closed-loop gain is

$$G_{cl} = \frac{\frac{k_j k_i (s + a_i)}{s^2 + sB_j}}{1 + \frac{k_j k_i (s + a_i)}{s^2 + sB_j}} = \frac{k_j k_i (s + a_i)}{s^2 + sB_j} \times \frac{s^2 + sB_j}{s^2 + sB_j + k_j k_i (s + a_i)} = \frac{k_j k_i (s + a_i)}{s^2 + (B_j + k_j k_i)s + k_j k_i a_i} \dots \dots 28$$

Comparing the closed-loop transfer function in Equation 14 to the second-order frequency equation gives rise to Equation 29.

$$\frac{k_j k_i (s + a_i)}{s^2 + (B_j + k_j k_i)s + k_j k_i a_i} = \frac{k_j k_i (s + a_i)}{s^2 + 2\zeta\omega_n s + \omega_n^2} \dots \dots 29$$

For the speed controller of this design, the natural frequency for the current loops is 2Hz while the damping factor was selected to be 0.707. $\omega_n = 2\pi f = 12.566\text{rad/s}$ and $\zeta = 0.707$. The torque constant is calculated as in Equation 30. Then k_j and B_j are calculated in Equations 31 and 32 respectively.

$$k_t = 3i_{sd}^* pp \frac{L_m^2}{l_r + L_m} = 3.528 \dots \dots 30$$

$$k_j = \frac{k_t}{J} = 342.530 \dots \dots 31$$

$$B_j = \frac{B}{J} = 0.015 \dots \dots \dots 32$$

Comparing denominators of Equation 29

$$s^2 + (0.015 + 342.53k_i)s + 342.53k_i a_i = s^2 + 17.769s + 12.566^2$$

$$s^1: 0.015 + 342.53k_i = 17.769$$

$$k_i = 0.052 \dots \dots \dots 32$$

$$s^0: 342.53k_i a_i = 12.566^2$$

$$a_i = 8.894 \dots \dots \dots 33$$

Therefore, from the controller block, proportional and integral are calculated as in Equations 22 and 23 respectively.

$$KP = k_i = 0.052 \dots \dots \dots 34$$

$$KI = k_i a_i = 0.461 \dots \dots \dots 35$$

Then, the speed controller gain becomes

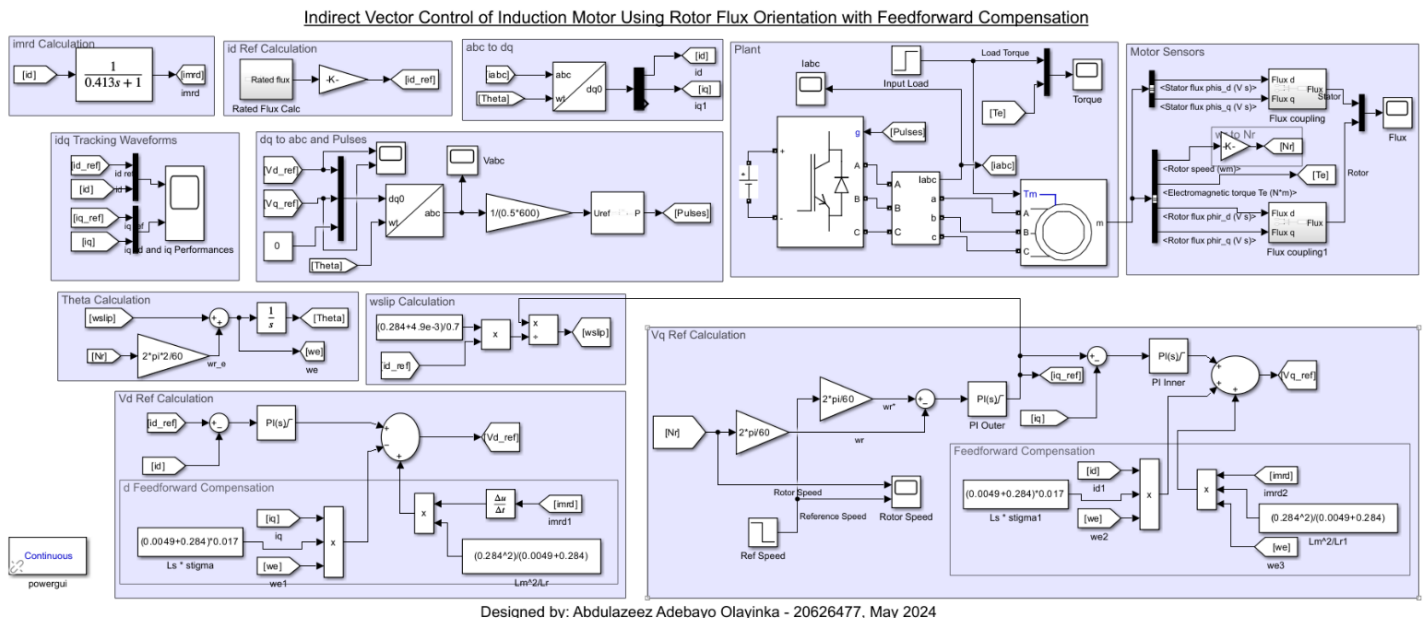
$$G_{ctrl} = \frac{0.052(s + 8.894)}{s}$$

IV. IMPLEMENTATION OF INDIRECT VECTOR CONTROL WITH FEEDFORWARD COMPENSATION

The calculated gains and their parameters in Section III were used to implement the circuit in Figure 2 with feedforward compensations (the third and fourth terms of Equations 3 and 4 respectively) on MATLAB Simulink as shown in Figure 5. The rated flux is calculated as in Equation 36 [8] which is implemented in the Simulink model (“Rated Flux Calc” subsystem). Then, the reference d-axis current is calculated in Equation 37 [2] [7], implemented in the Simulink Model (“id Ref Calculation” subsystem).

$$\varphi = \frac{V_{ph}}{4.44f} = 0.598 \text{ Wb} \dots \dots \dots 36$$

$$i_{sd}^* = \frac{\varphi}{L_m} = 2.106 \text{ A} \dots \dots \dots 37$$



Designed by: Abdulazeez Adebayo Olayinka - 20626477, May 2024

Figure 5: Model of Indirect Rotor Flux Orientation of Vector Control of the IM

The position is estimated with the speed slip equation in 38 and the “Theta Calculation” subsystem in the Model. The speed slip is calculated with Equation 39 [7] [9] [10] [11] which is implemented in the Simulink model environment of Figure 5 (“ωslip Calculation” subsystem).

$$\theta = \int (\omega_r + \omega_{slip}) dt \dots \dots \dots 38$$

$$\omega_{slip} = \frac{i_{sq}^*}{\tau_r i_{mrd}} \dots \dots \dots 39$$

Where i_{mrd} is the magnetising current which is constant and equal to the d-axis reference current because it is a constant flux operation and $\tau_r = \frac{l_r + L_m}{R_r} = 0.413sec$.

The inverter was fed with a 12kHz switching frequency to have fewer oscillations/ripples on the d and q currents and a 600Vdc was used as the inverter input voltage. The simulation was run for 1.2sec. the tracking of the d and q currents (i_{sd} and i_{sq}) with their respective reference values (i_{sd}^* and i_{sq}^*) is shown in Figure 6. There was a change in the q-axis reference current at 0.8sec due to a speed reference change at 0.8sec (Figure 7) and the q-axis current tracked this as expected.

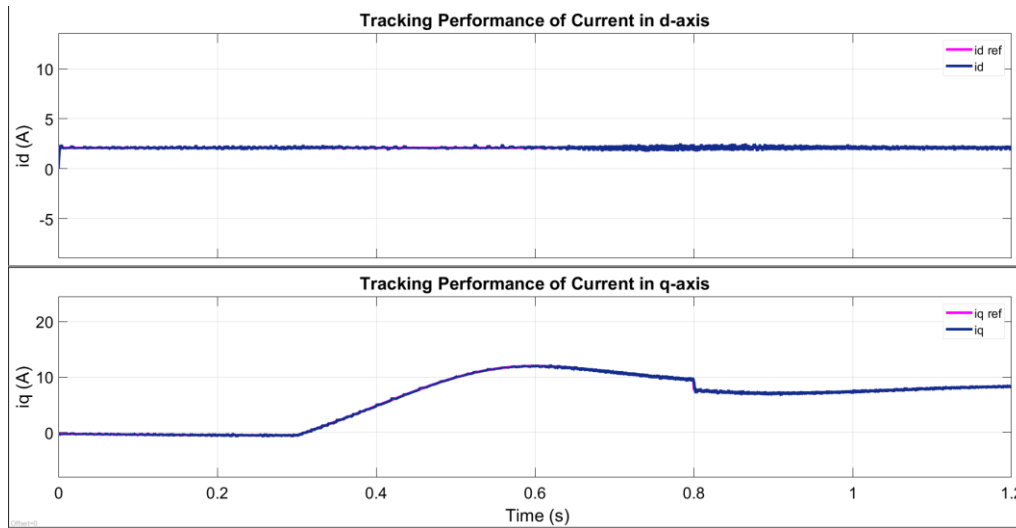


Figure 6: Tracking Performance of d and q Currents

To observe the tracking of the d-axis current (i_{sd}^*) with a change in the d-axis reference current (i_{sd}^*), i_{sd}^* was changed by a factor of 0.6 and the observed current tracking is shown in Figure 7.

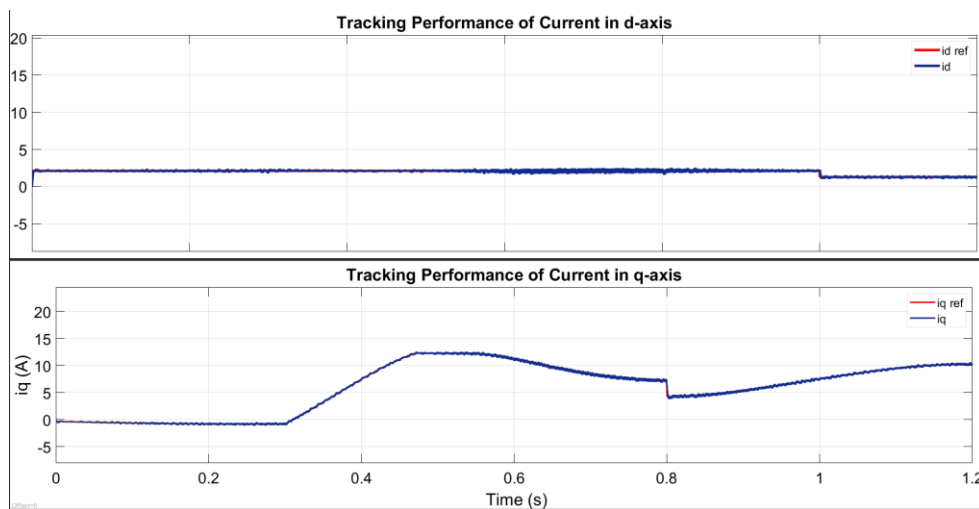


Figure 7: Tracking Performance of d and q Currents with a Change in i_{sd}^* and i_{sq}^*

The tracking performance for motor speed is shown in Figure 8. As can be seen, the motor needs about 0.4sec – 0.5sec after accelerating to settle at the reference speed of 1435rpm and a reduced speed to 900rpm at 0.8sec while a full load torque of 14.64Nm is applied at 0.3sec. The graph was exaggerated for visual purposes for the transient to be more appreciated. The simulation is then run for 8sec for the speed to be more settled as shown in Figure 9. The stator dynamics three-phase current, load and electromagnetic torques and stator and rotor flux are shown in these Figures (8 and 9).

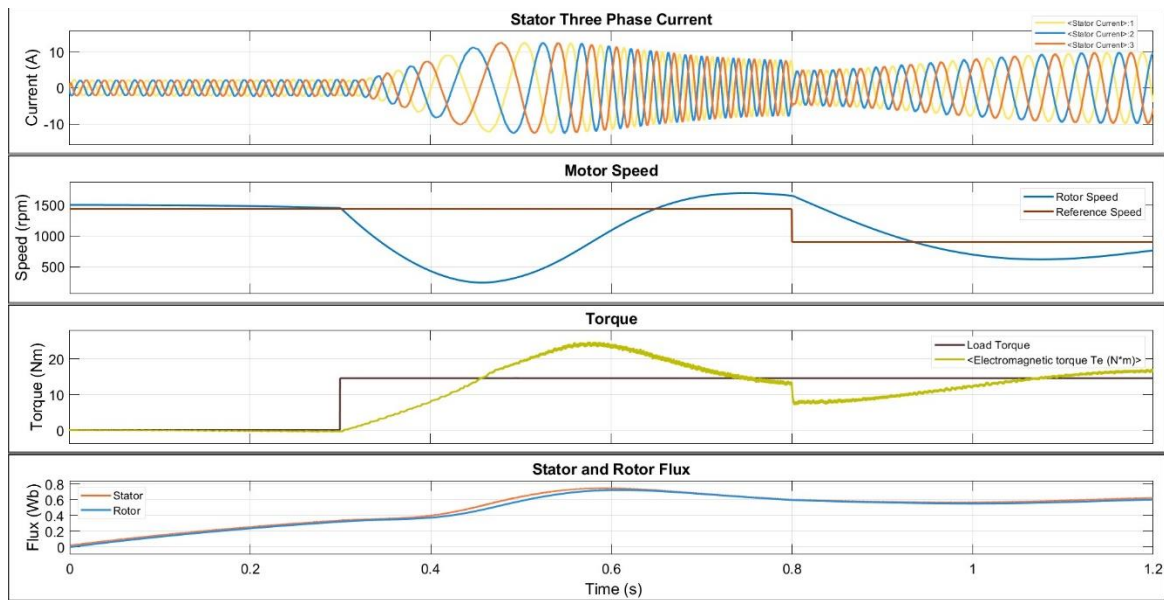


Figure 8: Current, Speed, Torque and Flux Plots

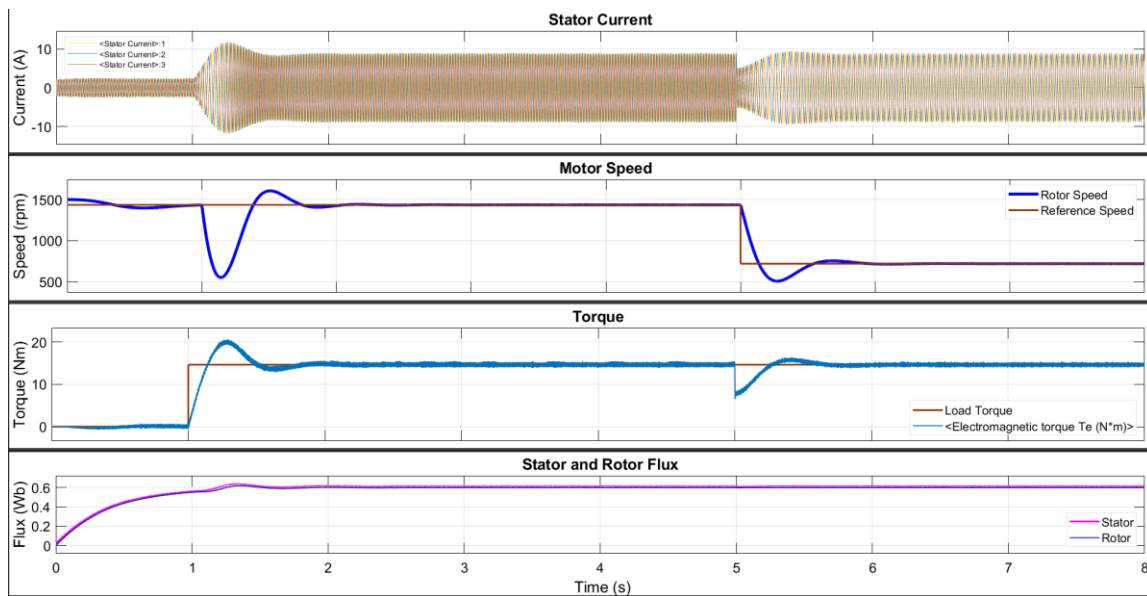


Figure 9: Current, Speed, Torque and Flux Plots – 8sec Simulation Time

• **Scalar Control vs Vector Control**

Scalar control observed in [1] was implemented with the following parameters and the same parameters were used to simulate the vector control on MATLAB Simulink. The motor parameters remain the same for this analysis.

Table II: Simulation Parameters

| Parameter | Initial Value | Final Value | Time to Step |
|-----------|---------------|-------------|--------------|
| Torque | 0 Nm | 14.64 Nm | 2 sec |
| Speed | 720 rpm | 1435 rpm | 2 sec |

It is observed that after the motor accelerates at no-load on scalar control, the motor speed never stabilises from 0 seconds to 2 seconds, likewise, electromagnetic torque and flux continue to oscillate about their respective values during this transient as shown in Figure 10. This is a result of no feedback from the output to the input because scalar control is an open-loop system, the scalar control needs load torque to balance the rotor Inertial. However, transitioning to full load was achieved at 720rpm and the rated speed was not achieved from the scalar control despite having fed in the rated voltage and frequency while suddenly changing to full load. This flux could not sustain the transient to the rated speed as it was operating at constant flux with no dynamic compensations. Stator currents are highly distorted during high starting currents.

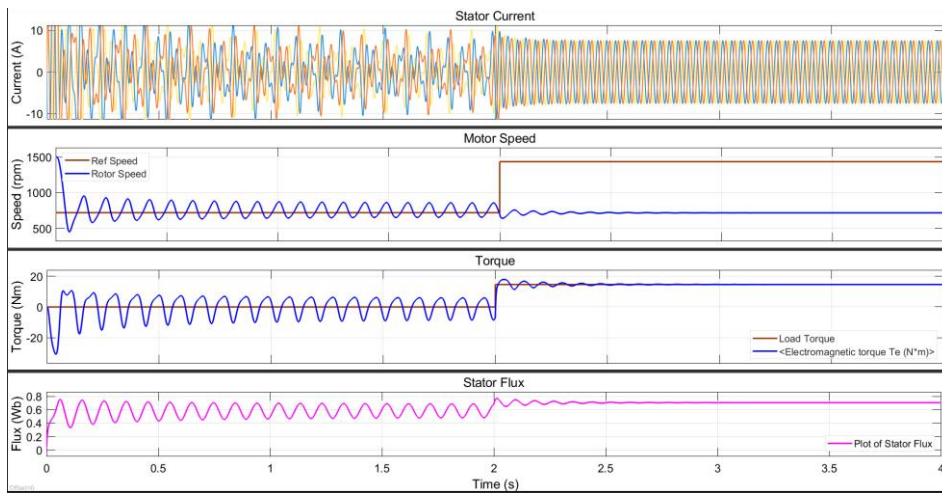


Figure 10: Scalar Control from Low-Speed (720rpm), No-load to Rated Speed (1435rpm), Full Load

Vector control, on the other hand, behaves very differently during these responses as it is a closed-loop system which ensures that the oscillation due to the acceleration either on no-load or at full-load rated speed stabilised after a few milliseconds. Figure 11 shows this response according to Table II simulation parameters. Hence, vector control is the best mode for controlling this induction motor with no visible high current distortion as compared to scalar control. There is a further discussion of this scalar vs vector control in Section VI.

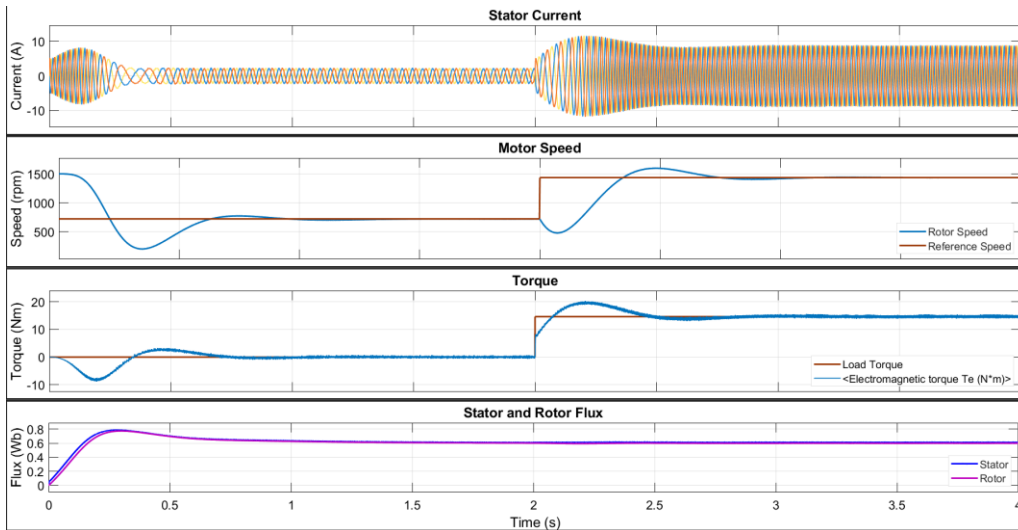


Figure 11: Vector Control of the IM Operating at 720rpm to 1435rpm

V. DESIGN IMPROVEMENT

A. Field Weakening Control

The field weakening allows the motor to operate at the speed above the rated value but reduces the field (flux) current in proportion to the increase in speed as shown in Equation 40. Hence the motor operated in the field weakening region, Figure 12. Figure 5 was tweaked to provide operation in the field weakening region as implemented on Simulink.

$$i_{sdnew}^* = \frac{N_{rated}}{N_{ref}} i_{sd}^* \dots \dots \dots 40$$

A “Field Weakening” subsystem and “IF” statement switch block were added to the model in Figure 5 to be able to perform field weakening if the reference speed is above the rated speed as in Equation 40, the system modelling is shown in Figure 13. This functionality will ensure the model can be used for both Section IV and V (Field Weakening Control). Therefore, a single Simulink model is submitted for this report as the model is further modified for online rotor constant estimation which will be discussed in the next subsection.

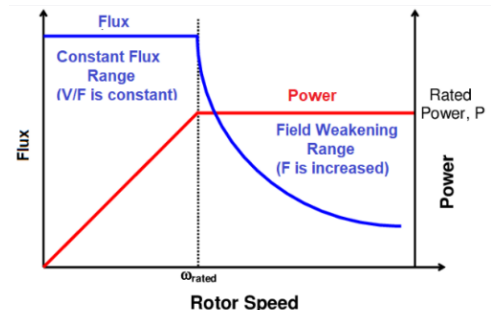


Figure 12: Field Weakening

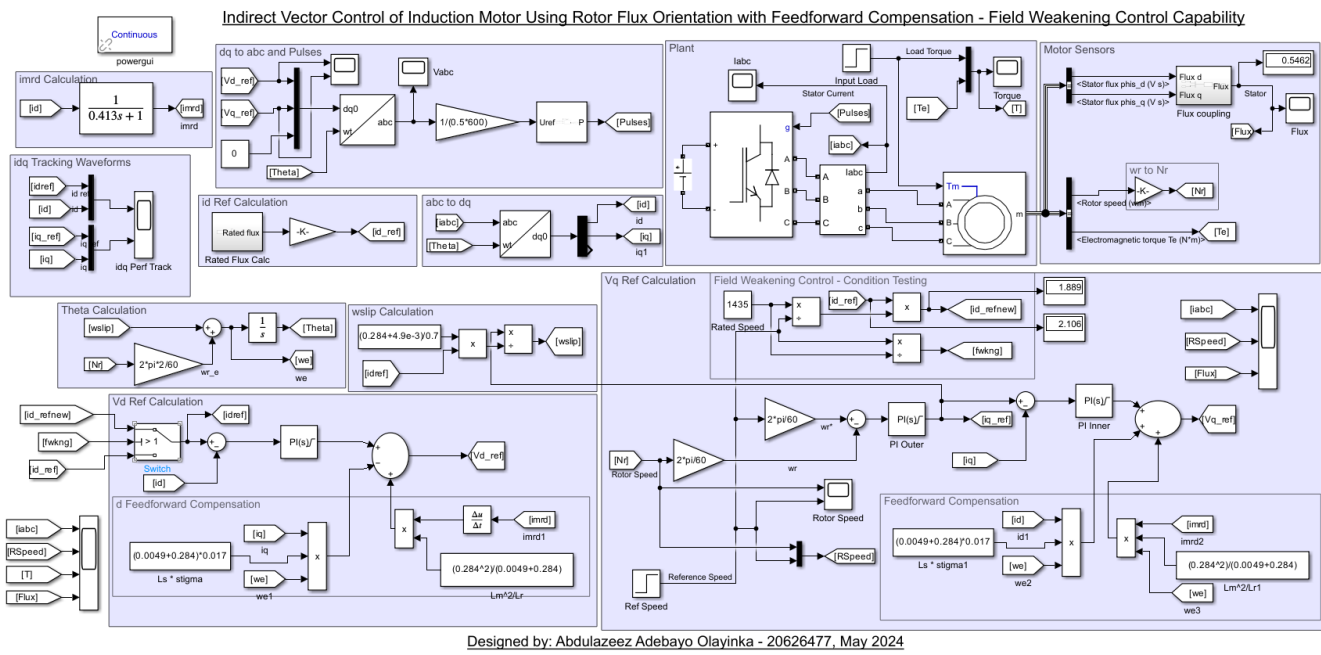


Figure 13: Indirect Vector Control Model with Field Weakening Capability

The model was simulated with a reference speed of 1435rpm starting from no-load to sudden transition to full load at 1sec and continued to 2s where a sudden reference speed transition to 1800rpm. It was observed that the actual rotor speed tracked this reference speed as shown in Figure 14. The stator current increases as the flux reduces with the proportion of the increase in the reference speed.

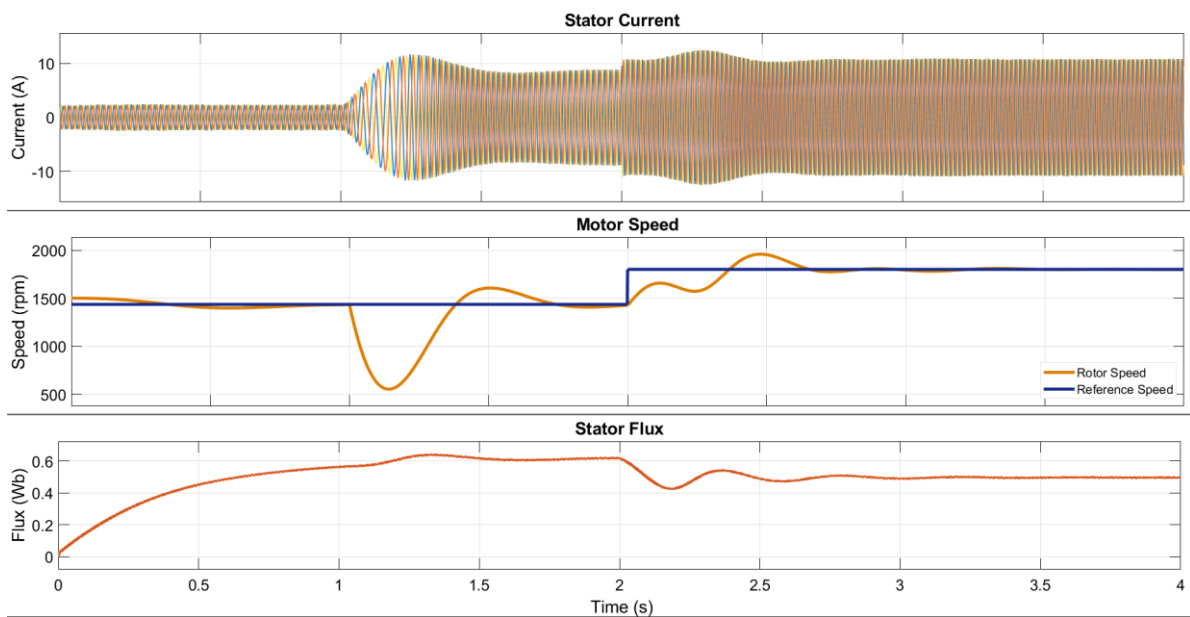


Figure 14: Field Weakening Stator Current, Speed and Flux Plots

The d-axis and q-axis current plots where the currents track their respective reference values are shown in Figure 15. The waveform (plot) is exaggerated for a proper visual of the dynamic, the same test conditions and dynamics of Figure 14 are also applied to this current tracking performance.

The limitations of field weakening include

- i. **Stability and Reliability:** the flux may be reduced below the flux required to overcome collapses
- ii. **Reduced Torque:** the torque will reduce as speed increases to maintain a constant power
- iii. **Increased Current and Losses:** overall current will increase causing heat loss and insulation breakdown
- iv. **Voltage Limitations:** voltage cannot be increased beyond the supply voltage hence increase in current to maintain constant power

v. Motor Design Considerations.

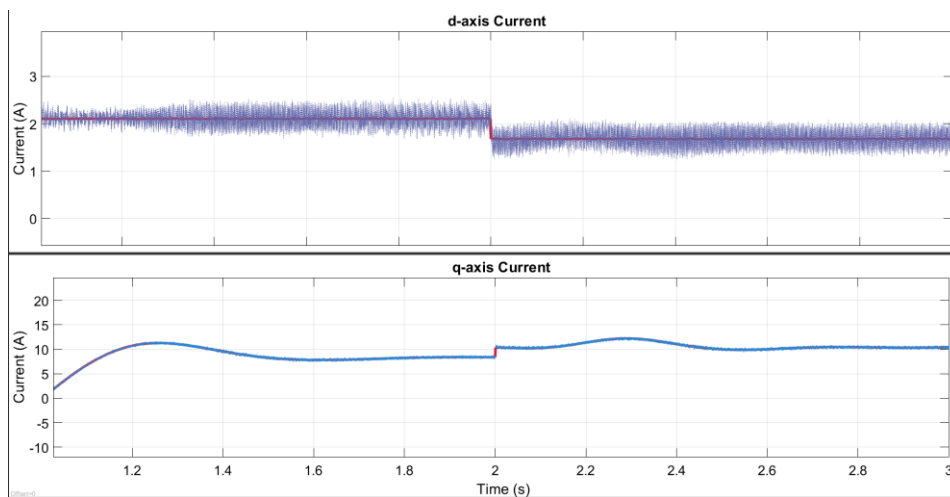


Figure 15: Tracking Performance of dq Currents Under Field Weakening Condition

B. Parametric Drift Through Variation in Rotor Resistance – Online Rotor Time Constant

The rotor time constant (RTC), determined by rotor resistance and rotor inductance, suffers from considerable variation over time due to the thermal drift and saturation effects [12] [13], as shown in Equation 39 position is largely dependent on the accuracy of the rotor time constant. Hence, a need to improve the design by considering this variation to have an online rotor time constant estimation should the rotor resistance change or erroneous calculation from steady-state analysis in [1]. The simulations performed in this section were run at full load, rated speed.

Let the machine's actual rotor resistance be set at 1.2Ω and the data available in [1] was used to estimate the rotor time constant as in previous sections of this report, the simulation was run on these bases. Figure 16 shows the observed system dynamics with motor speed (reference and rotor), slip speed and stator flux without revised rotor time constant. Due to the increase in rotor resistance, the flux was observed to overshoot the rated during the motor acceleration by about a 200% increase and stayed at about 0.9Wb when the motor settled which is 0.3Wb (50% above-rated flux). Also, during starting of the IM, i_{sq}^* could not follow the i_{sq} during the initial transient.

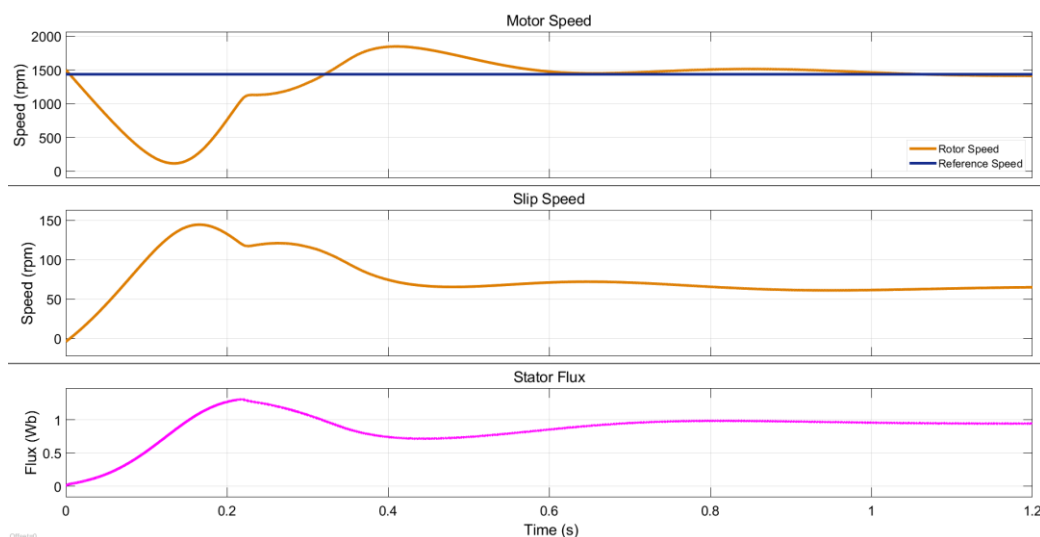


Figure 16: Incorrect Rotor Time Constant - Speed, Slip Speed and Stator Flux

To overcome this incorrect rotor time constant which can lead to performance error in the drive, the online rotor time constant is employed to revise this inputted rotor time constant. There are several methods available in estimating the online rotor time constant such as Model Reference Adaptive System (MRAS) using dot product of stator current and rotor flux by [14], online parameter estimation method based on steady-state voltage model by [12], a Q-based MRAS method was adopted by [15] to mention but a few methods of this online estimation of rotor constant. However, the method employed by [13] was implemented for this design.

From the dynamic equation of the rotor, the rotor voltage equation can be obtained [13]:

$$0 = R_r i_{rd} + \frac{d}{dt} \varphi_{rd} \dots \dots 41$$

$$0 = R_r i_{rq} + \frac{d}{dt} \varphi_{rq} \dots \dots 42$$

Based on the above equations, the variation in rotor resistance can be obtained [13]:

$$\widehat{R}_r = \sqrt{\frac{\left(\frac{d\varphi_{rd}}{dt}\right)^2 + \left(\frac{d\varphi_{rq}}{dt}\right)^2}{(i_{rd})^2 + (i_{rq})^2}} \dots \dots 43$$

Then, the rotor time constant can be obtained from Equation 44 while substituting Equation 43.

$$\widehat{\tau}_r = \frac{L_r}{\widehat{R}_r} \dots \dots 44$$

After substituting Equation 43 into Equation 44, the online estimator of the rotor constant was implemented in the model in Figure 13 with the addition of the following subsystem, Figure 17.

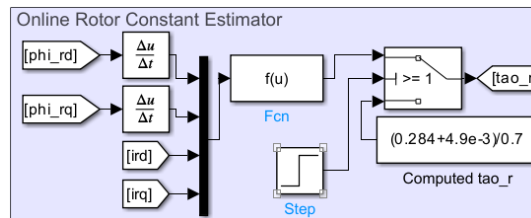


Figure 17: Online Rotor Time Constant Estimator

The simulation was run for 4sec with the rotor time constant computer with the parameters in Table I for 1.8sec, the same dynamics in Figure 16 were observed for this period. The online rotor time constant was imposed at 1.8sec and the dynamics changes as shown in Figure 18. The motor behaves with normal operations as observed in section IV with the stator flux drifting to its rated value and steady after a few milliseconds due to acceleration/deceleration in the slip speed. The parametric drift of rotor resistance was achieved with the actual machine rotor constant.

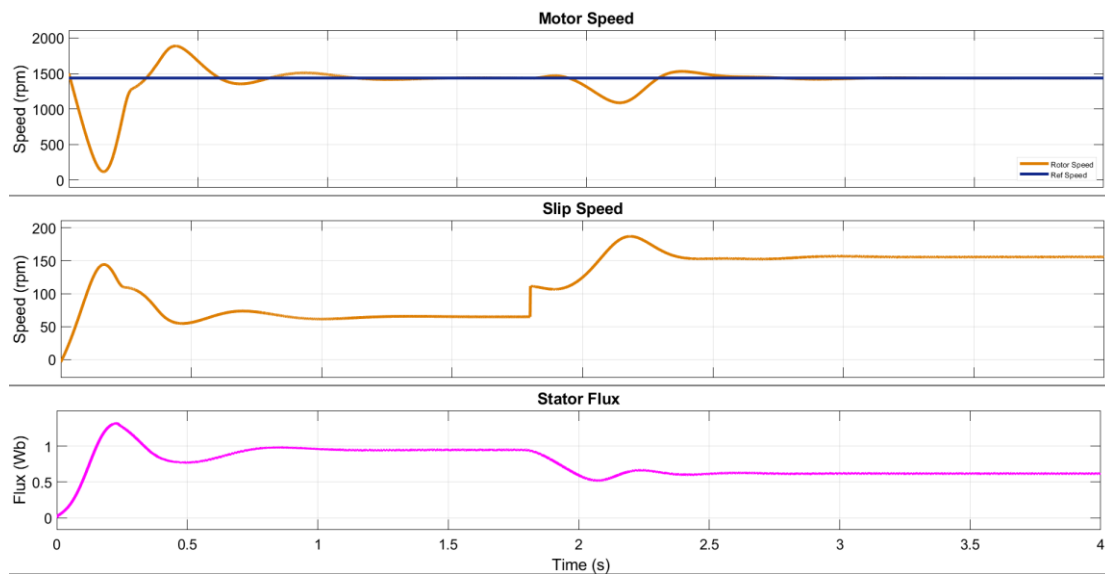


Figure 18: Rotor Time Constant based on Online Estimation – RTC Revised

The d-axis and q-axis currents were tracking their respective references during this revised rotor time constant is given in Figure 19. With incorrect rotor resistance, the q-axis current was low while during the revised estimated resistance the current increased, this indicates that the machine's actual rotor resistance was higher than the one used for estimation in Sections III and IV.

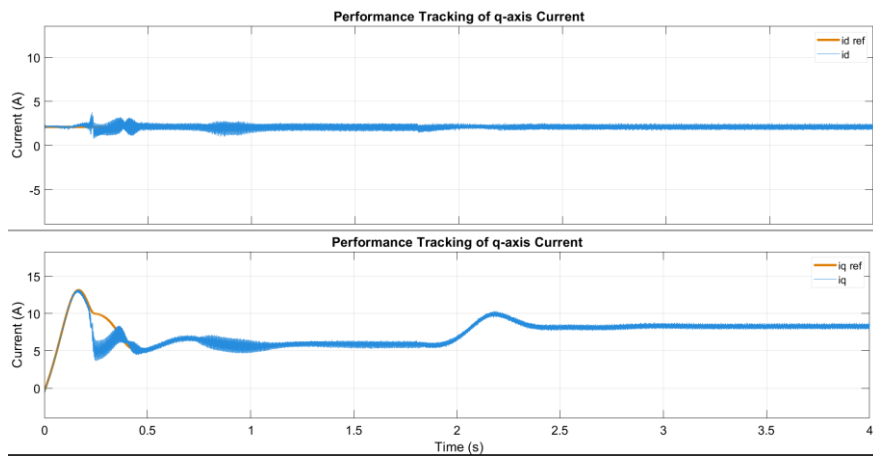


Figure 19: Current Tracking in the dq Reference Frame with the Respective Reference Values – Revised RTC

The estimated online rotor resistance is equal to the machine rotor resistance set above which is 1.2Ω as shown in Figure 20.

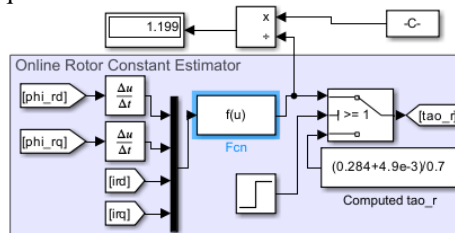


Figure 20: Online Rotor Time Constant with the Rotor Resistance Value being Displayed

VI. FURTHER DISCUSSION

The full system design for all the functions of the vector control requirement for this design is shown in Figure 21. These functionalities include - indirect vector control of the motor drive with feed-forward compensation, field weakening control and parametric drift in rotor time constant control.

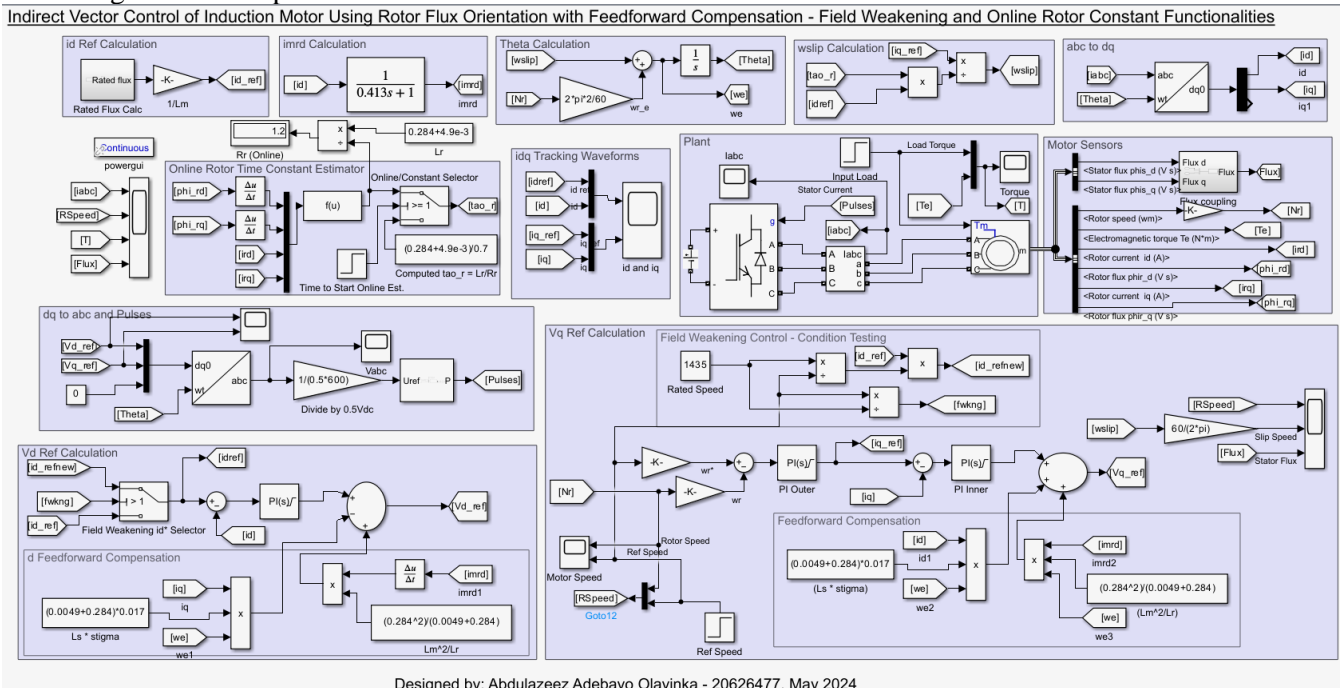


Figure 21: Indirect Vector Control of the Motor Drive with Feed-forward Compensation Model

The model was simulated to capture the system dynamics of the motor speed, slip speed, stator flux, torque and stator current as shown in Figures 22 and 23 respectively under the online rotor time constant estimation and field weakening. The online rotor time constant corrected the wrongly calculated rotor resistance at 1sec as the high flux goes back to 0.6Wb rated while the slip speed increases as the rotor resistance increases to its machine value. It can be seen that this model works according to the requirement and has a good tracking performance.

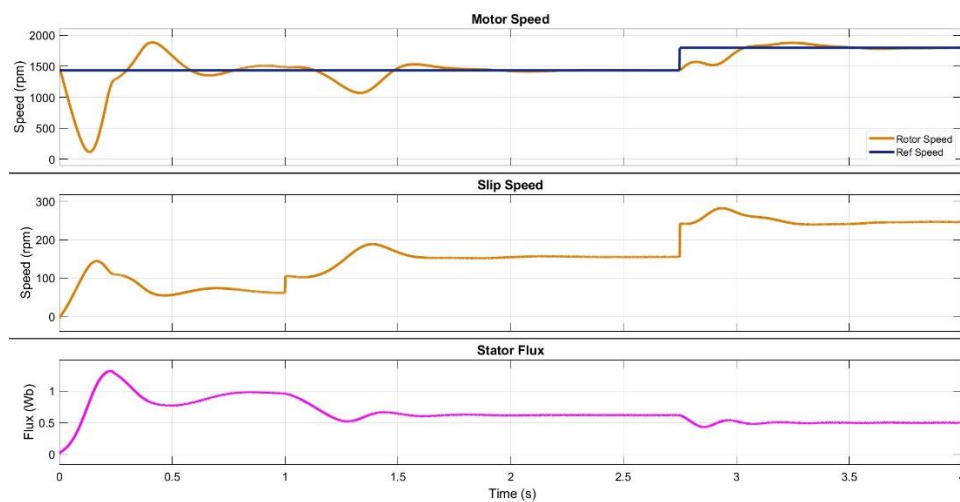


Figure 22: Performance Operation of the Indirect Vector Control of the IM - Motor Speed, Slip Speed and Stator Flux

As the speed increases to 1800rpm, the stator current also increases in this proportion to maintain the constant power while the flux reduces in the same proportion. The load torque remains constant because the input was set to the rated torque hence the reason for the increase in input power through the stator current and voltage.

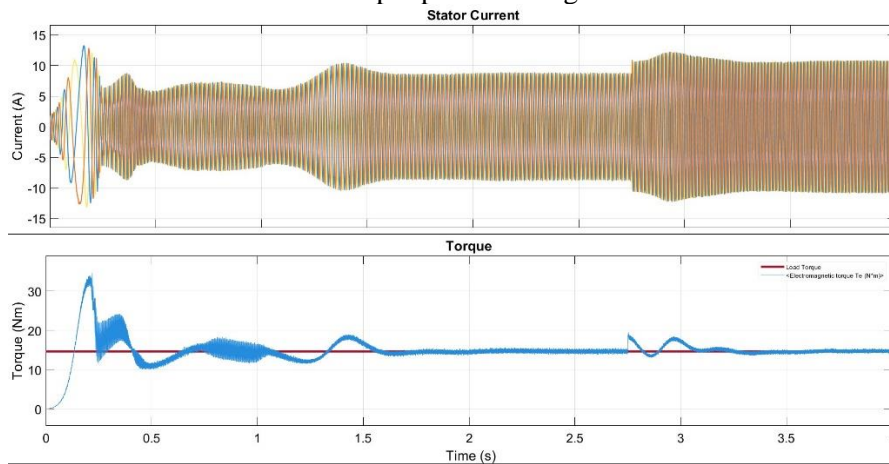


Figure 23: Tracking the performance of dq Currents in Full Operation of the Motor

All these complex functionalities are easily implemented on vector control without causing any long-term instability to the system which cannot be easily achievable in scalar control as the motor flux will either collapse causing large oscillation in the motor dynamics or speed changes may not be achieved at the desired times.

Vector Control (Indirect Rotor Flux Orientation):

- Advantages:
 - Superior Speed Control: offers precise and independent control of motor speed and torque, Figure 22. This is achieved by decoupling the torque-producing and flux-generating components of the stator current
 - High Performance: enables faster response times, improved transient performance, and better regulation at low speeds compared to scalar control
 - Wide Speed Range: can operate the motor over a wider speed range, including near-synchronous speeds, Figure 18
 - Improved Efficiency: can potentially achieve higher motor efficiency by optimizing the magnetic field within the motor.
- Disadvantages:
 - Complexity: requires more complex control algorithms, sensors (rotor speed sensor is often needed), and computational power compared to scalar control, Figure 21
 - Cost: additional complexity translates to higher implementation costs compared to scalar control
 - Tuning: tuning the control system can be more involved compared to scalar control.

Scalar V/f Control:

- Advantages:

- Simplicity: Employs a simple control scheme based on adjusting the voltage-to-frequency ratio (v/f) supplied to the motor [1]
- Low Cost: Easier and cheaper to implement due to the simplicity of the control scheme and minimal sensor requirements (often only a stator current sensor).
- Easy to Use: Requires minimal tuning compared to vector control.
- Disadvantages:
 - Limited Speed Control: offers less precise speed control, especially at low speeds and during transient conditions, Figure 10
 - Lower Performance: Slower response times and poorer regulation compared to vector control, Figure 10
 - Narrow Speed Range: effective speed control is limited to a smaller range, typically below the rated speed [1]
 - Lower Efficiency: may operate at lower efficiency due to suboptimal control of the magnetic field.

VII. CONCLUSION

In this paper, the indirect vector control of the motor was implemented and the currents in both d and q reference frames have a very good performance tracking in all the functionalities of this drive as observed in the simulation results. The rotor speed also tracked the reference speed with a good performance. The transient conditions of this vector control have better settling time as compared to scalar control.

This investigation explored the implementation of online rotor time constant estimation for indirect vector control of an induction motor in Simulink. The approach utilized the rotor flux observer to dynamically estimate the rotor time constant. The field weakening control was also implemented which allowed the motor to be operated above its rated speed while maintaining constant power.

REFERENCES

- [1] T. N. M. Abdulazeez Adebayo Olayinka, "Designing of an Induction Motor Drive and Controller," University of Nottingham, Nottingham, 2024.
- [2] T. N. Mir, Writer, *Coursework: Advanced AC Drives (EEEE 4114) 2023-24*. [Performance]. University of Nottingham, 2024.
- [3] T. M. U. W. P. R. Ned Mohan, *Power Electronic -*, New York: John Wiley & Sons Inc., 1995.
- [4] P. M. S. PERDIGÃO, *Power Electronics Lecture Note STEPS 2023*, Coimbra: Polytechnic Institute of Coimbra, 2023.
- [5] *STGB10NC60KD, STGD10NC60KD STGF10NC60KD, STGP10NC60KD*. [Film]. United Kingdom: STMicroelectronics Group of Companies, 2009.
- [6] RS, "STMicroelectronics STGP10NC60KD IGBT, 20 A 600 V, 3-Pin TO-220, Through Hole," [Online]. Available: <https://uk.rs-online.com/web/p/igbts/1686468?gb=s>. [Accessed 13 04 2024].
- [7] A. Walker, *EEEE4114: Advanced AC Drives*, Nottingham: University of Nottingham, 2024.
- [8] A. E. Fitzgerald, C. Kingsley and S. D. Umans, *Electric Machinery*, McGraw-Hill, 2003.
- [9] B. K. Bose, *Modern Power Electronics and AC Drives*, New Jersey: Prentice-Hall Inc., 2002.
- [10] R. Krishna, *Electric Drives, Modelling, Analysis and Control*, New Jersey: Prentice-Hall Inc., 2001.
- [11] E. Undeti and M. Chakravarthy, "The Control of Three-Phase Squirrel Cage Induction Motor by Indirect Field Oriented Control for E-Mobility," in *International Conference on Emerging Frontiers in Electrical and Electronic Technologies (ICEFEET)*, Patna, India, 2023.
- [12] J. Zhang, J. Chai, X. Sun and H. Lu, "On-line parameter estimation for indirect field oriented control of induction machine based on steady state voltage model," in *IECON 2014 - 40th Annual Conference of the IEEE Industrial Electronics Society - IEEE Xplore*, Dallas, TX.
- [13] W. Gao, "A simple model-based online rotor time constant estimator for an induction machine," *IEEE Transactions on Energy Conversion*, vol. 19, no. 4, pp. 793 - 794, 2004.
- [14] X. Zhang, Y. Zhang, S. Yang, Z. Xie and P. Cao, "An Improved MRAS for Rotor Time Constant Updating in Induction Motor Drives Utilizing Dot Product of Stator Current and Rotor Flux," *IEEE Transactions on Power Electronics*, vol. 34, no. 9, pp. 8905 - 8915, 2019.
- [15] H. Kim, Y. Han and K. Lee, "Improved Q-MRAS Based Online Rotor Time Constant Compensation for IFOC Induction Motor Drives," in *2023 IEEE Applied Power Electronics Conference and Exposition (APEC)*, Orlando, FL, 2023.